LUND UNIVERSITY

The Intratumoral Distribution of Radiolabeled 177Lu-BR96 Monoclonal Antibodies Changes in Relation to Tumor Histology over Time in a Syngeneic Rat Colon Carcinoma Model.

Örbom, Anders; Eriksson, Sophie; Elgström, Erika; Ohlsson, Tomas G; Nilsson, Rune; Tennvall, Jan; Strand, Sven-Erik

Published in:
Journal of Nuclear Medicine

DOI:
10.2967/jnumed.112.117028

2013

Link to publication

Citation for published version (APA):
Örbom, A., Eriksson, S., Elgström, E., Ohlsson, T. G., Nilsson, R., Tennvall, J., & Strand, S-E. (2013). The Intratumoral Distribution of Radiolabeled 177Lu-BR96 Monoclonal Antibodies Changes in Relation to Tumor Histology over Time in a Syngeneic Rat Colon Carcinoma Model. *Journal of Nuclear Medicine*, *54*(8), 1404-1410. https://doi.org/10.2967/jnumed.112.117028

Total number of authors:
7

General rights
Unless other specific re-use rights are stated the following general rights apply:
Copyright and moral rights for the publications made accessible in the public portal are retained by the authors and/or other copyright owners and it is a condition of accessing publications that users recognise and abide by the legal requirements associated with these rights.
• Users may download and print one copy of any publication from the public portal for the purpose of private study or research.
• You may not further distribute the material or use it for any profit-making activity or commercial gain
• You may freely distribute the URL identifying the publication in the public portal

Read more about Creative commons licenses: https://creativecommons.org/licenses/

Take down policy
If you believe that this document breaches copyright please contact us providing details, and we will remove access to the work immediately and investigate your claim.

LUND UNIVERSITY

PO Box 117
221 00 Lund
+46 46-222 00 00

The Intratumoral Distribution of Radiolabeled ^{177}Lu-BR96 mAbs Changes in Relation to Tumor Histology over Time in a Syngeneic Rat Colon Carcinoma Model

Anders Örbom*[1], Sophie E. Eriksson*[2], Erika Elgström[2], Tomas Ohlsson[1], Rune Nilsson[2], Jan Tennvall[2,3] and Sven-Erik Strand[1]

[1]Department of Medical Radiation Physics, Lund University, Lund, Sweden, [2]Department of Oncology, Lund University, Lund, Sweden and [3]Department of Oncology, Skåne University Hospital, Lund, Sweden

* Contributed equally to this work.

Author correspondence to: Anders Örbom, Medical Radiation Physics, Lund University, Barngatan 2:1, SE-22185 Lund, Sweden, Tel: +46 46 222 0839, Fax: +46 46 178 540, E-mail: anders.orbom@med.lu.se

Both principal authors are graduate students pursuing their PhDs.

Word count: 5795

Financial support: This research was supported by grants from the Swedish Research Council, the Swedish Cancer Society, Mrs. Berta Kamprad's Foundation, Gunnar Nilsson's Foundation, The Crafoord Foundation, Government Funding of Clinical Research within the

National Health Service, King Gustaf V's Jubilee Foundation, the Lund University Medical Faculty Foundation, The Eurostars program through the Swedish Governmental Agency for Innovation Systems (VINNOVA) and The Lund University Hospital Fund.

Running title: Intratumoral temporal distribution of ^{177}Lu-mAbs

Abstract

The therapeutic effect of radioimmunotherapy depends on the distribution of the absorbed dose in relation to viable cancer cells within the tumor, which in turn is a function of the activity distribution. The aim of this study was to investigate the distribution of ^{177}Lu-DOTA-BR96 monoclonal antibodies (mAbs) targeting the Lewis Y antigen over 7 days using a syngeneic rat model of colon carcinoma.

Methods: 38 tumor bearing rats were given 25 or 50 MBq/kg body weight ^{177}Lu-DOTA-BR96 i.v. and were sacrificed 2, 8, 24, 48, 72, 96, 120, or 168 h post-injection (p.i.) with activity measured in blood and tumor samples. Adjacent cryosections of each tumor were analyzed in three ways: imaging using a silicon-strip detector for digital autoradiography, staining for histological characterization, or staining to determine the distribution of the antigen, vasculature and proliferating cells using immunohistochemistry. Absorbed-dose rate distribution images at the moment of sacrifice were calculated using the activity distribution and a point-dose kernel. The correlations between antigen expression and both activity uptake and absorbed-dose rate were calculated for several regions of interest in each tumor. Nine additional animals with tumors were given unlabeled antibody to evaluate possible immunological effects.

Results: At 2-8 h p.i. the activity was found in the tumor margins, at 24 h p.i. in viable antigen-expressing areas within the tumor, and at 48 h p.i. and later increasingly in antigen-negative areas of granulation tissue. The correlation between antigen expression and both the mean activity and absorbed-dose rate in regions of interest, changed from positive to negative after 24 h p.i. Antigen-negative areas also increased over time in animals injected with unlabeled BR96 compared to untreated tumors.

Conclusion: The results indicate that viable Lewis Y-expressing tumor cells are most efficiently treated during the initial uptake period. The activity then seems to remain in these

initial uptake regions after the elimination of tumor cells and formation of granulation tissue. Further studies using these techniques could aid in determining the effects of the intratumoral activity distribution on overall therapeutic efficacy.

Keywords: Radioimmunotherapy; autoradiography; dosimetry; intratumoral heterogeneity, Lutetium-177

INTRODUCTION

The limited success of radioimmunotherapy against solid tumors can be partly attributed to the difficulty in achieving high tumor uptake and penetration of radiolabeled monoclonal antibodies (mAbs) (*1, 2*). Aspects of the microenvironment of solid tumors that limit the distribution of antibodies throughout viable regions include abnormal vasculature, high interstitial fluid pressure and impaired lymphatic drainage (*3-5*), as well as the composition of the extracellular matrix (*6, 7*). The antibody characteristics are also important for the microdistribution; for example, high-affinity antibodies risk entrapment in perivascular regions at a "binding site barrier" (*8, 9*), and those targeting an intracellular antigen preferentially collect in necrotic areas (*10, 11*). Additionally, during the time of antibody uptake, the tumor is a dynamic system with regard to treatment effects, repopulation, and angiogenesis, all of which can affect antibody distribution (*12*).

Colorectal carcinoma is the third most common cancer in humans (*13*) and is prone to metastasize (*14*), which makes it suitable for systemic treatment strategies like radioimmunotherapy. Several preclinical studies have been performed on the intratumoral distribution of antibodies, primarily targeting carcinoembryonic antigen (CEA) in immune-deficient mice bearing subcutaneous xenografts of human colorectal cancers (*15-20*). However, such xenografts are artificial tumor models with little interaction with the host, e.g. with a low probability of metastasizing, and with stromal and vascular interactions not similar to human cancers (*21*). To better mimic the clinical situation, our group has established a syngeneic rat model of colon carcinoma for radioimmunotherapy using the mAb BR96 that targets the tumor-associated antigen Lewis Y (Le^y) (*22*). For labeling we used Lutetium-177 ($T_{½}$=6.73 days) which is both a beta (79% $E_{\beta max}$=498 keV, 12% $E_{\beta max}$=177 keV, 9% $E_{\beta max}$=385 keV) and gamma (10% E_{γ}=208 keV, 6% E_{γ}=113 keV) emitter.

In this study we investigated the distribution of the radiolabeled antibody within tumors at different time points up to 7 days post-injection (p.i.) in relation to histology, antigen expression and vascularization. We also calculated the intratumoral absorbed-dose rate distribution at the time of sacrifice in relation to the same factors.

MATERIALS AND METHODS

Monoclonal Antibody

The chimeric (mouse/human) monoclonal IgG1 antibody BR96 (Seattle Genetics Inc., Seattle, WA) binds to the tumor-associated antigen Le^y. Several human carcinoma types express Le^y, including breast, gastrointestinal tract, pancreas, non-small-cell lung, cervical and ovarian cancers. BR96 also binds to some normal tissues, mainly epithelial cells of the gastrointestinal tract (*23*). The dissociation constant (K_d) is 4 nM (*22*).

Radioimmunoconjugate

BR96 was conjugated with the DOTA chelate (S-2-(4-isothiocyanatobenzyl)-1,4,7,10-tetraazacyclododecane tetraacetic acid; Macrocyclics, Dallas, TX) as previously described (*22*). The number of DOTA moieties per BR96 molecule was determined by matrix-assisted laser desorption ionization mass spectroscopy (MALDI-MS). The antigen-binding properties (immunoreactivity) of DOTA-BR96 relative to BR96 were determined by saturation binding curve analysis, using BN7005 cells as the target antigen. The immunoreactivity is given by the ratio: K_d(BR96)/K_d(DOTA-BR96).

The following procedure was used for labeling with $^{177}LuCl_3$ (MDS Nordion, Vancouver, Canada). Both the DOTA-BR96 conjugate in 0.25 M ammonium acetate buffer and the radionuclide solution were preheated at 45°C for 10 min. The DOTA-BR96 solution was then

added to the radionuclide-containing vial and incubated at 45°C for 15 min. The reaction was quenched with an excess of DTPA for 5 min and diluted in 1% human serum albumin (HSA, Baxter Medical AB, Kista, Sweden). The radiochemical purity of the labeled immunoconjugate was determined by instant thin-layer chromatography (ITLC) using a 1 x 9 cm silica-gel-impregnated fiberglass sheet, eluted in 0.1 M EDTA. Separation by size-exclusion chromatography together with high-performance liquid chromatography (HPLC) (7.8 x 300 mm molecular sieving column, Phenomenex SEC S3000; Phenomenex, Torrance, CA, eluted in 0.05 M sodium phosphate at 1.0 mL/min) was used to determine the radiochemical purity and to detect signs of aggregation or fragmentation.

Rat Tumor Model

Immunocompetent male Brown Norway (BN) rats (n=38 for the main study; Harlan, Horst, the Netherlands) with a mean body weight of 214 g (SD 24 g) at the time of tumor cell inoculation were used. These animals express BR96-binding antigen in some normal tissues, mainly in the epithelium of the gastrointestinal tract (*24*). The animals were housed under standard conditions with standard pellets and fresh water *ad libitum*. All experiments were conducted in compliance with Swedish legislation on animal protection, and were approved by the regional ethics committee on animal experiments.

BN7005-H_1D_2 is a rat colon carcinoma cell line established from a 1,2-dimethylhydrazine-induced tumor from a BN rat. The fraction surviving 2 Gy at high absorbed-dose rate *in vitro* (S_{2Gy}) is 0.5 for this cell line (unpublished data). The cells were cultured in RPMI-1640 medium with stable glutamine supplemented with 10% fetal bovine serum (both from PAA Laboratories GmbH, Pasching, Austria), 1 mM sodium pyruvate, 10 mM Hepes buffer, and 14 µg/mL Gentamicin (all from Gibco Invitrogen, Carlsbad, CA) at 37°C, in a humidified environment containing 5% CO_2. Cells were washed with PBS, detached by trypsin treatment

and resuspended in supplemented medium. The animals were inoculated between the peritoneum and the abdominal wall with 3 x 10^5 cells under anesthesia (Isoflurane, Abbott Scandinavia AB, Solna, Sweden).

Study Design and Biodistribution

The main study was conducted as two separate experiments referred to as Group 1 and Group 2 (Table 1). Tumors were measured and volumes were calculated as length x width^2 x 0.4, as previously established (*25*), at injection of the radioimmunoconjugate and at 72-168 h p.i. At 13-14 days post-inoculation 150 µg of ^{177}Lu-DOTA-BR96 (in 0.4 mL PBS with 1% HSA) was injected via a tail vein. The administered activity of ^{177}Lu-DOTA-BR96 was 50 MBq/kg body weight in Group 1 and 25 MBq/kg body weight in Group 2. A lower activity was administered to Group 2 to reduce possible radiation-induced cytotoxic effects in the tumors and samples were taken at different time points to observe changes in activity distribution. Arterial blood samples were drawn 2 min p.i. and before sacrifice for activity measurements in a NaI(Tl) well counter (Group 1: 1282 Compugamma CS; LKB Wallac, Turku, Finland; Group 2: Wallac Wizard 1480, PerkinElmer, Shelton, CT). Animals were euthanized 2, 8, 24, 48, 72, 96, 120 and 168 h p.i., and the tumors were excised and cut in half. One half was embedded in Tissue-Tek® O.C.T.™ compound (Sakura Finetek, Zoeterwoude, the Netherlands) and frozen on dry ice, and the activity of the other half was measured in a NaI(Tl) well counter. The frozen samples were cryosectioned, starting at the tumor center. Sections used for autoradiography were 20 µm (Group 1) or 30 µm (Group 2) thick. Sections used for staining were 10 µm thick and stored at -80°C.

Control of Antibody Effects

In order to evaluate untreated tumor histology and antigen expression and the therapeutic effects of the unlabeled antibody, 18 rats were inoculated with tumor cells as described above.

Tumors from 9 untreated rats were excised on the day corresponding to antibody injection. The remaining 9 rats were injected with 0.1, 1.0 or 10.0 mg/kg unlabeled BR96 (n=3/group) and sacrificed 48 h p.i. The tumors were fixed in 4% paraformaldehyde and paraffin embedded before sectioning and staining for histology and antigen expression.

Digital Autoradiography

The ^{177}Lu activity distribution was imaged using microscope slides containing 3 tumor sections per slide. These were imaged for 10 hours each, using a double-sided silicon strip detector with an intrinsic spatial resolution of 50 µm (Biomolex 700 Imager, Biomolex AS, Norway). The recorded coordinates of all detected event were analyzed using IDL 6.4 software (ITT Visual Information Solutions, Boulder, CO). Corrections were applied for dead or miscalibrated strips, and for radioactive decay.

To determine the detector efficiency for each section thickness, adjacent tumor sections were imaged and their activity measured in the NaI(Tl) well counter for quantification of all tumor section images. The total mass of the sections on each slide was calculated by the section thickness times the density (1.0 g/cm^3) times the area determined from histology stainings. Images were scaled to percent injected activity per gram (%IA/g) using the mass, the total activity per section and the decay-corrected injected activity. Visualization and region-of-interest (ROI) based analysis of the images were performed using ImageJ software (*26*). Six ROIs (0.1-4.5 mm^2 in size) were drawn on one tumor section per animal; two regions each outlining structures visually identified as having high, medium and low levels of activity uptake relative to the entire section.

Dosimetry

In order to calculate the absorbed-dose rate distribution in tumor sections at the time of sacrifice, a point-dose kernel (PDK) (*27*) for ^{177}Lu was generated with the Monte Carlo code

MCNP5 1.4 (*28*) utilizing the new electron transport logic (dbcn 17j 2). The PDK was modeled as concentric spheres with radii increasing in steps of 100 µm inside a 2.1 mm diameter cube in a tissue-equivalent medium (1.00 g/cm^3). Simulations included beta particles, gamma rays, conversion electrons, and Auger electrons emitted at the origin, with the energy deposition tallied in each layer. One imaged section per tumor was used. Each image was normalized to the activity at the time of sacrifice and stacked to form a new three-dimensional dataset with the shortest diameter matching that of the PDK. The volume was down-sampled to cubic voxels with 100 µm sides before convolution with the PDK. The resulting absorbed-dose rate image was then extracted from the middle of the stack. Mean absorbed-dose rate for the whole section and in ROIs corresponding to those in the activity image were quantified.

Histology and Immunohistochemistry

After autoradiography, the sections used for detection and adjacent sections were stained with Mayer's Hematoxylin and Chromotrope 2R (both from Histolab AB, Gothenburg, Sweden). Sections were stained for the detection of antigen expression (BR96), blood vessel distribution (RECA-1, Abcam plc, Cambridge, UK) and proliferation (anti-Ki67 clone SP6, Thermo Fisher Scientific Inc., Fremont, CA). The slides were dried for 15 min at 37°C and then fixed either for 8 min with 4% phosphate-buffered formalin (Histolab AB, for antigen and proliferation staining) or for 5 min in ice-cold acetone (for staining of blood vessels). The sections were then washed with TRIS-buffered saline with Tween 20, pH 7.4 and blocked of endogenous peroxidases by Peroxidase blocking solution (Dako, Glostrup, Denmark), before the addition of primary antibodies. All antibodies were diluted in Antibody Diluent (Dako). Slides were incubated with the primary antibodies either overnight (BR96 and RECA-1) or for 2 h (SP6) in a moist chamber at room temperature. After washing, secondary antibodies were added to the slides. The secondary antibodies used were peroxidase-conjugated donkey

anti-human IgG for the detection of BR96, peroxidase-conjugated donkey anti-mouse IgG for the detection of RECA-1, and peroxidase-conjugated donkey anti-rabbit IgG for the detection of SP6 (all from Jackson ImmunoResearch Laboratories Inc. West Grove, PA). Slides were incubated for either 3 h (BR96 and RECA-1) or 1 h (SP6) in a moist chamber at room temperature. After washing, diaminobenzidine (Dako) was added before hematoxylin staining (1 min) and subsequent dehydration and mounting.

Areas corresponding to the ROIs were exported as individual images from adjacent sections stained for the detection of antigen expression, and processed to suppress blue cell nuclei staining. The ratio of stained to non-stained areas in each image was then calculated using Aperio ImageScope software (Aperio Technologies, Vista, CA) and the Positive Pixel Count v9 algorithm. Algorithm parameters were calibrated separately per group of animals due to different staining intensities. (Supplemental Fig. 1).

Statistical Analysis

To test the image quantification, the values of the mean %IA/g obtained from the digital autoradiography images were compared to the corresponding values from NaI(Tl) well counter measurements for the same tumors using a paired-samples t-test. The activities measured by well counter for animal Groups 1 and 2 were also compared at each time point p.i., using the nonparametric independent-samples Mann-Whitney U test. The Pearson correlation between the antigen staining ratio and the activity uptake, as well as the estimated absorbed-dose rate in the ROIs was calculated at each time point that had data from at least 5 animals, i.e. 30 ROIs. Normal distribution was assumed in this test due to the number of samples. All analyses were performed with IBM SPSS Statistics version 19 (SPSS Inc., Chicago, IL); $p < 0.05$ being considered significant.

RESULTS

Radioimmunoconjugation

The mean number of DOTA molecules per IgG was determined to be 2.4. The immunoreactivity was given by the ratio of the dissociation constant for BR96 and DOTA-BR96, and was found to be 0.86, which was not significantly different from unlabeled BR96. The specific activity used for Group 1 was 86 MBq/mg, the radiochemical purity according to ITLC was >99%, and no aggregates or fragments were observed with HPLC. The specific activity used for Group 2 was 42.5 MBq/mg, the radiochemical purity was >97.5%, and 1.3% labeled aggregated fraction according to HPLC.

Biodistribution

Biodistribution data for blood and tumors are presented in Table 2. Pharmacokinetic analysis of the decay-corrected %IA/g for blood resulted in a t½α of 5.6 h and t½β of 32.5 h (nonlinear regression, two-phase decay, GraphPad Prism 5.04). The mean tumor volume at injection was 650 mm^3 (SD 235 mm^3) and the median tumor uptake was 8.4 %IA/g (range 6.3-9.8 %IA/g) at 48 h p.i., after which there were increased variations in uptake and tumor volumes. Of the 18 tumors excised 72 h or later, three had continued to grow, four had minor changes in volume, and 11 had decreased in size. No statistically significant difference in tumor %IA/g could be found between the two groups of animals at any time point p.i. using a nonparametric test. No significant difference that would indicate a systematic error in image quantification was found between tumor activity uptake measured by well counter or by quantitative autoradiography.

Absorbed-Dose Rate at Moment of Sacrifice

Images of the absorbed-dose rate distributions were produced from digital autoradiography images. The intratumoral absorbed-dose rate distribution closely mimics the activity distribution (Fig. 1) as most of the energy is deposited close to the point of decay. Table 3 shows the median values and ranges for the mean absorbed-dose rate over the entire section are presented for each time point and animal group.

Activity Distribution in Comparison to Tumor Histology, Antigen Expression and Vascularization

At 2 and 8 h p.i., the radioactivity was mainly distributed close to viable and antigen-positive tumor margins (Fig. 1A). The stainings showed dense tumor growth with necrotic areas at the center of the tumors. All tumors were well vascularized, contained a high proportion of proliferating cells, and the Le^y antigen was detectable on almost all viable tumor cells. At 24 h p.i., the activity had penetrated into the more central areas of the tumor sections, however, higher levels were still observed peripherally in half of the evaluated tumors. The areas with high activity correlated mainly to antigen-positive areas in the viable regions (Fig. 1B). Tumors were well vascularized and some also had small areas of granulation tissue. At 48 h p.i., there was a change in histology compared to untreated controls (Fig. 2A, B), with areas of granulation tissue that overlapped activity hot spots in 5 of 6 tumors (Fig. 1C). Areas with low activity had high levels of available antigen and blood vessels were detected in all areas. At 72-168 h p.i., the activity distribution varied between the individual tumors; ranging from local areas of high activity to a more homogeneous distribution. Tumors that decreased in size after the mAb injection contained few blood vessels and few proliferative cells, whereas the opposite was observed for the tumors that continued to grow. Small tumors had fewer antigen-positive cells and a larger proportion of stroma or granulation tissue, often with high activity uptake, while larger tumors had dense areas of tumor cells and intense staining of the

antigen, typically with limited uptake (Fig. 1D). There was no notable uptake in the necrotic areas over the time observed.

Control of Antibody Effects

Tumor cells from untreated animals all had complete membrane staining for the Le^y antigen (Fig. 2B). The low BR96 dose of 0.1 mg/kg resulted in small areas of unstained tumor cells close to the tumor margins. Both 1.0 and 10.0 mg/kg led to limited antigen staining and altered histology, including the formation of granulation tissue and necrosis, while untreated and low dose animals all showed dense growth of tumor cells with occasional areas of necrosis (Fig. 2).

Region of Interest Analysis

The mean activity per gram, the mean absorbed-dose rate at the time of sacrifice, and the percentage of the area stained as antigen-positive were calculated for each ROI. The absorbed-dose rate in the high uptake regions (Table 3) was found to be approximately twice as high as the mean absorbed-dose rate for the whole section. The results of the Pearson correlation analysis of the relationships between activity uptake and absorbed-dose rate, and the antigen-positive area are given in Table 4. The correlation coefficient changed over time, from positive at 8 and 24 hours p.i. to negative from 48 h p.i. and onwards (Fig. 3). Activity uptake and absorbed-dose rate exhibited very similar correlations with antigen though the correlation with absorbed-dose rate was stronger at earlier than at later time points.

DISCUSSION

The results of this study show the dynamic process of intratumoral antibody distribution in a syngeneic animal model, and also how heterogeneous distribution results in a considerable

variation in the absorbed-dose rate. Initially, the activity was localized to the periphery of the tumor, presumably near perfused blood vessels, followed by a comparatively homogeneous distribution corresponding to viable antigen-expressing tumor tissue at 24 h p.i. The subsequent trend of increasing correlation between activity uptake and granulation tissue was interpreted as the effect of treatment, reducing viable, antigen-positive tumor cells in areas with high activity uptake. Activity uptake does not necessarily infer antibody uptake, since it is not known whether the radionuclide was still coupled to the mAb or free after degradation, or if the mAb was intact or fragmented. The ROI-based analysis showed a negative correlation between antigen expression and activity uptake from 48 h p.i. and onwards. This correlation was stronger than that reported previously by Flynn *et al*. (*16*) who based their results on a pixel-by-pixel correlation between CEA and antibody in a subcutaneous xenograft. While the methods of analysis differ, it is also likely to be an effect of the differences in antigen expression, vascularization and immune response between the animals used (*17*). The increased variance in tumor uptake after 48 h p.i. was attributed to variations in tumor growth or reduction, as has been observed elsewhere (*19*). The new cell populations present in several tumors had little activity uptake, probably due to lower antibody concentration in the blood. This increased variance is likely more evident in syngeneic animal tumor models, which often show a faster rate of proliferation compared to human tumors (*21*). No correlation was apparent between individual tumor growth or reduction and intratumoral activity distribution in this study.

Starting at 24 h p.i., the histological properties of the tumors changed from predominantly proliferative tumor cells to areas of granulation tissue, concurrent with a decrease in tumor volumes. In order to study the mAb distribution separately from radio-therapeutic effects, the administered activities were lower than those needed for clinical response according to our previous work (*22*). Therefore, these effects may be due to an immunological response

mediated via the Fc region of the antibodies (*29, 30*). This is supported by the presence of granulation tissue in tumors from animals treated with unlabeled BR96 but not in untreated controls. At therapeutic activities of ^{177}Lu (400 MBq/kg), the decrease in peripheral leukocytes (*22*) probably results in an impaired immune response. Instead, with absorbed-dose rates and total absorbed doses approximately 8 times higher than in this study, radiation-induced cell death might dominate in achieving complete response (*31*).

Calculations of absorbed-dose rate distributions at different time points showed that high-uptake regions are exposed to twice the absorbed-dose rate compared to the whole tumor section mean. Estimating the accumulated mean tumor absorbed doses over several days from the calculated absorbed-dose rates showed that they would fall in the area of several grays at late time points, absorbed doses leading to the majority of cells dying if given at a single instant in an in vitro assay. However, the low ^{177}Lu activity and absorbed-dose rate in this study may allow the tumor to repair DNA damage and repopulate by proliferation of undamaged or restored cells. The correlation between viable, antigen-expressing tissue and areas of relatively high absorbed-dose rate at 24 h p.i. indicates that using a longer-range beta emitter such as ^{90}Y would not necessarily increase tumor cell death at therapeutic activities. In contrast, the concentration of activity in areas of granulation tissue and stroma at later times suggests that a radionuclide with a shorter half-life than that used in the present study would be more beneficial. Further studies, particularly at therapeutic activity levels, are needed to fully evaluate the effects of the intratumoral temporal activity distribution on the efficacy of radioimmunotherapy in relation to radionuclide half-life and emission properties.

Earlier studies using models of colorectal cancer in immune-deficient mice show limited agreement with our observations of activity accumulation in granulation and stromal tissue at later time points. Two studies report the uptake of ^{125}I-labeled anti-CEA antibody in necrotic areas at 48 h p.i. and onwards, although this is most likely an effect of free antibody or iodine

pooling in blood (*16, 19*). Studies of anti-CEA antibodies in subcutaneous xenografts of well differentiated and regularly vascularized tumors exhibited a similar pattern of uptake to that in our model, while the antibody never penetrated very far from the blood vessels in poorly differentiated and vascularized tumors (*17*). Observations of another antibody, A33, in a well-differentiated model also showed early uptake around blood vessels resulting in homogeneous tumor uptake by 48 h p.i. (*15*). Anti-CEA antibodies had penetrated well-vascularized intrahepatic xenografts effectively at 24 h p.i. (*18-20*), which is more in agreement with our results, compared with subcutaneous tumors of the same cell line (*17, 32*). Lower-affinity antibodies (e.g. anti-HER2) penetrate tumors more efficiently (*9*), and modeling predicts that binding-site barrier effects are unlikely for mAbs with K_d>1 nM (*33*), such as BR96 (K_d=4 nM). The observed reduction in tumor cell density around 24-48 h p.i. could also affect the activity distribution since apoptosis-inducing pretreatment has been shown to increase the rate and extent of antibody penetration (*12, 34*).

CONCLUSION

The results of this study show the initial process of antibody penetration into viable antigen-expressing tumor areas over approximately 24 hours, followed by a decreasing association between activity uptake and viable, antigen-expressing tumor tissue over a period of several days. This indicates that delivering a high absorbed-dose rate during the initial penetration and uptake period is especially important for a therapeutic response.

ACKNOWLEDGEMENTS

We would like to thank Dr. Erik Larsson (Medical Radiation Physics, Lund University) for performing the simulation of the point-dose kernel, Dr. Peter Senter (Seattle Genetics, Inc.) for kindly providing the BR96 mAb, and Dr. Otto Ljungberg (Dept. of Pathology, Skåne University Hospital, Malmö) for excellent help with histological evaluations. This research was supported by grants from the Swedish Research Council, the Swedish Cancer Society, Mrs. Berta Kamprad's Foundation, Gunnar Nilsson's Foundation, The Crafoord Foundation, Government Funding of Clinical Research within the National Health Service, King Gustaf V's Jubilee Foundation, the Lund University Medical Faculty Foundation, The Eurostars program through the Swedish Governmental Agency for Innovation Systems (VINNOVA), and The Lund University Hospital Fund.

REFERENCES

1. Jain M, Venkatraman G, Batra SK. Optimization of radioimmunotherapy of solid tumors: biological impediments and their modulation. *Clin Cancer Res.* 2007;13:1374-1382.

2. Huang CY, Pourgholami MH, Allen BJ. Optimizing radioimmunoconjugate delivery in the treatment of solid tumor. *Cancer Treat Rev.* 2012;38:854-860

3. Minchinton AI, Tannock IF. Drug penetration in solid tumours. *Nat Rev Cancer.* 2006;6:583-592.

4. Beckman RA, Weiner LM, Davis HM. Antibody constructs in cancer therapy: protein engineering strategies to improve exposure in solid tumors. *Cancer.* 2007;109:170-179.

5. Tabrizi M, Bornstein GG, Suria H. Biodistribution mechanisms of therapeutic monoclonal antibodies in health and disease. *AAPS J.* 2010;12:33-43.

6. Netti PA, Berk DA, Swartz MA, Grodzinsky AJ, Jain RK. Role of extracellular matrix assembly in interstitial transport in solid tumors. *Cancer Res.* 2000;60:2497-2503.

7. Choi J, Credit K, Henderson K, et al. Intraperitoneal immunotherapy for metastatic ovarian carcinoma: Resistance of intratumoral collagen to antibody penetration. *Clin Cancer Res.* 2006;12:1906-1912.

8. Fujimori K, Covell DG, Fletcher JE, Weinstein JN. A modeling analysis of monoclonal antibody percolation through tumors: a binding-site barrier. *J Nucl Med.* 1990;31:1191-1198.

9. Rudnick SI, Lou J, Shaller CC, et al. Influence of affinity and antigen internalization on the uptake and penetration of Anti-HER2 antibodies in solid tumors. *Cancer Res.* 2011;71:2250-2259.

10. Smith-Jones PM, Vallabhajosula S, Navarro V, Bastidas D, Goldsmith SJ, Bander NH. Radiolabeled monoclonal antibodies specific to the extracellular domain of prostate-specific membrane antigen: preclinical studies in nude mice bearing LNCaP human prostate tumor. *J Nucl Med.* 2003;44:610-617.

11. Ruggiero A, Holland JP, Hudolin T, et al. Targeting the internal epitope of prostate-specific membrane antigen with 89Zr-7E11 immuno-PET. *J Nucl Med.* 2011;52:1608-1615.

12. Jang SH, Wientjes MG, Lu D, Au JL. Drug delivery and transport to solid tumors. *Pharm Res.* 2003;20:1337-1350.

13. Ferlay J SH, Bray F, Forman D, Mathers C and Parkin DM. GLOBOCAN 2008 v1.2, Cancer Incidence and Mortality Worldwide: IARC CancerBase No. 10. http://globocan.iarc.fr. Accessed June 13, 2012.

14. Hess KR, Varadhachary GR, Taylor SH, et al. Metastatic patterns in adenocarcinoma. *Cancer.* 2006;106:1624-1633.

15. Antoniw P, Farnsworth AP, Turner A, et al. Radioimmunotherapy of colorectal carcinoma xenografts in nude mice with yttrium-90 A33 IgG and Tri-Fab (TFM). *Br J Cancer.* 1996;74:513-524.

16. Flynn AA, Boxer GM, Begent RH, Pedley RB. Relationship between tumour morphology, antigen and antibody distribution measured by fusion of digital phosphor and photographic images. *Cancer Immunol Immunother.* 2001;50:77-81.

17. El Emir E, Qureshi U, Dearling JL, et al. Predicting response to radioimmunotherapy from the tumor microenvironment of colorectal carcinomas. *Cancer Res.* 2007;67:11896-11905.

18. Fidarova EF, El-Emir E, Boxer GM, et al. Microdistribution of targeted, fluorescently labeled anti-carcinoembryonic antigen antibody in metastatic colorectal cancer: implications for radioimmunotherapy. *Clin Cancer Res.* 2008;14:2639-2646.

19. Dearling JL, Flynn AA, Qureshi U, et al. Localization of radiolabeled anti-CEA antibody in subcutaneous and intrahepatic colorectal xenografts: influence of tumor size and location within host organ on antibody uptake. *Nucl Med Biol.* 2009;36:883-894.

20. Frampas E, Maurel C, Remaud-Le Saec P, et al. Pretargeted radioimmunotherapy of colorectal cancer metastases: models and pharmacokinetics predict influence of the physical and radiochemical properties of the radionuclide. *Eur J Nucl Med Mol Imaging.* 2011;38:2153-2164.

21. Workman P, Aboagye EO, Balkwill F, et al. Guidelines for the welfare and use of animals in cancer research. *Br J Cancer.* 2010;102:1555-1577.

22. Eriksson SE, Ohlsson T, Nilsson R, Tennvall J. Repeated radioimmunotherapy with 177Lu-DOTA-BR96 in a syngeneic rat colon carcinoma model. *Cancer Biother Radiopharm.* 2012;27:134-140.

23. Hellstrom I, Garrigues HJ, Garrigues U, Hellstrom KE. Highly tumor-reactive, internalizing, mouse monoclonal antibodies to Le(y)-related cell surface antigens. *Cancer Res.* 1990;50:2183-2190.

24. Sjogren HO, Isaksson M, Willner D, Hellstrom I, Hellstrom KE, Trail PA. Antitumor activity of carcinoma-reactive BR96-doxorubicin conjugate against human carcinomas in athymic mice and rats and syngeneic rat carcinomas in immunocompetent rats. *Cancer Res.* 1997;57:4530-4536.

25. Badn W, Kalliomaki S, Widegren B, Sjogren HO. Low-dose combretastatin A4 phosphate enhances the immune response of tumor hosts to experimental colon carcinoma. *Clin Cancer Res.* 2006;12:4714-4719.

26. Rasband WS. ImageJ. http://imagej.nih.gov/ij/, 2012.

27. Roeske JC, Aydogan B, Bardies M, Humm JL. Small-scale dosimetry: challenges and future directions. *Semin Nucl Med.* 2008;38:367-383.

28. X-5 Monte Carlo Team. MCNP - A General Monte Carlo N-Particle Transport Code, Version 5, Volume I: Overview and theory, Los Alamos National Laboratory report LA-UR-03-1987. 2003 (revised 2/1/2008).

29. Ferris RL, Jaffee EM, Ferrone S. Tumor antigen-targeted, monoclonal antibody-based immunotherapy: clinical response, cellular immunity, and immunoescape. *J Clin Oncol.* 2010;28:4390-4399.

30. Houot R, Kohrt HE, Marabelle A, Levy R. Targeting immune effector cells to promote antibody-induced cytotoxicity in cancer immunotherapy. *Trends Immunol.* 2011;32:510-516.

31. Song H, Sgouros G. Radioimmunotherapy of solid tumors: searching for the right target. *Curr Drug Deliv.* 2011;8:26-44.

32. Rhoden JJ, Wittrup KD. Dose dependence of intratumoral perivascular distribution of monoclonal antibodies. *J Pharm Sci.* 2012;101:860-867.

33. Wittrup KD, Thurber GM, Schmidt MM, Rhoden JJ. Practical theoretic guidance for the design of tumor-targeting agents. *Methods Enzymol.* 2012;503:255-268.

34. Jang BS, Lee SM, Kim HS, et al. Combined-modality radioimmunotherapy: synergistic effect of paclitaxel and additive effect of bevacizumab. *Nucl Med Biol.* 2012;39:472-483.

Figures

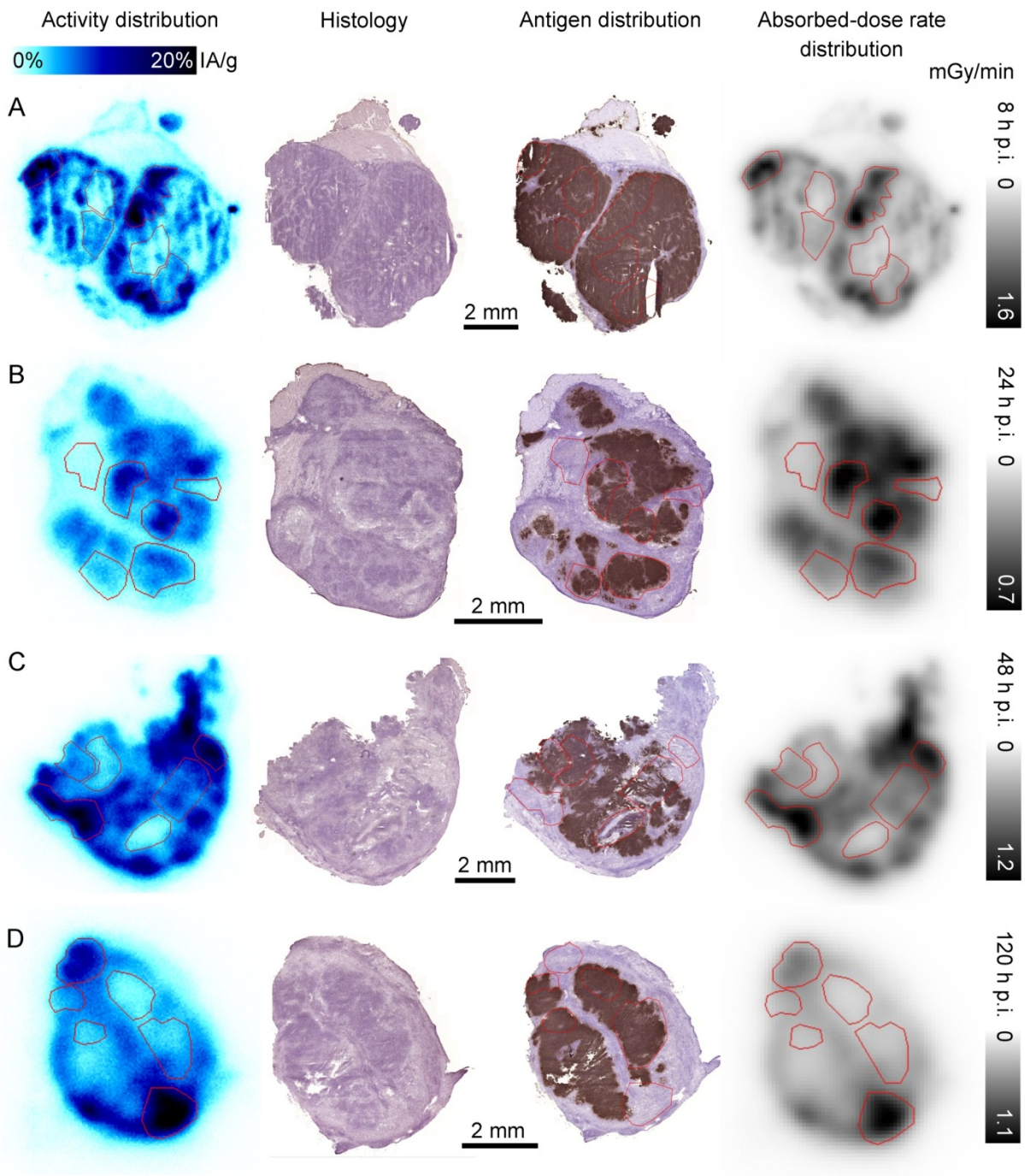

FIGURE 1. Representative tumor sections from Group 2 at four points in time p.i. From left to right: the digital autoradiography image of ^{177}Lu distribution scaled to %IA/g, followed by adjacent sections stained with hematoxylin and eosin for histological examination, and with BR96 antibody to determine antigen distribution, and finally the absorbed-dose rate

distribution at the time of sacrifice based on the activity image (individually scaled). Regions of interest used in correlation analysis are outlined in red where applicable. Sections from Group 2 are displayed due to the visually better quality staining for antigen distribution. Note the peripheral distribution of activity in each nodule at 8 h p.i. (A), and the correlation between uptake and antigen at 24 h p.i. (B), which at 48 h p.i. (C) has given way to a correlation between activity and antigen-negative granulation tissue, which is even more pronounced at 120 h p.i. (D).

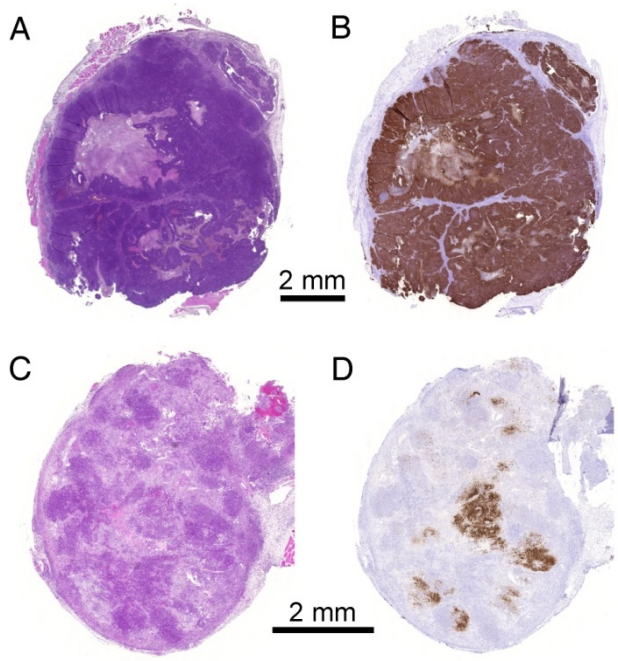

FIGURE 2. Representative tumor sections from untreated animals (top) and animals treated with 1.0 mg/kg of unlabeled mAb 48 h p.i. (bottom). The images show sections stained with hematoxylin and eosin (A and C) and with BR96 antibody (B and D). Note the reduction in viable, antigen-expressing tumor cells in the tumor treated with unlabeled mAb.

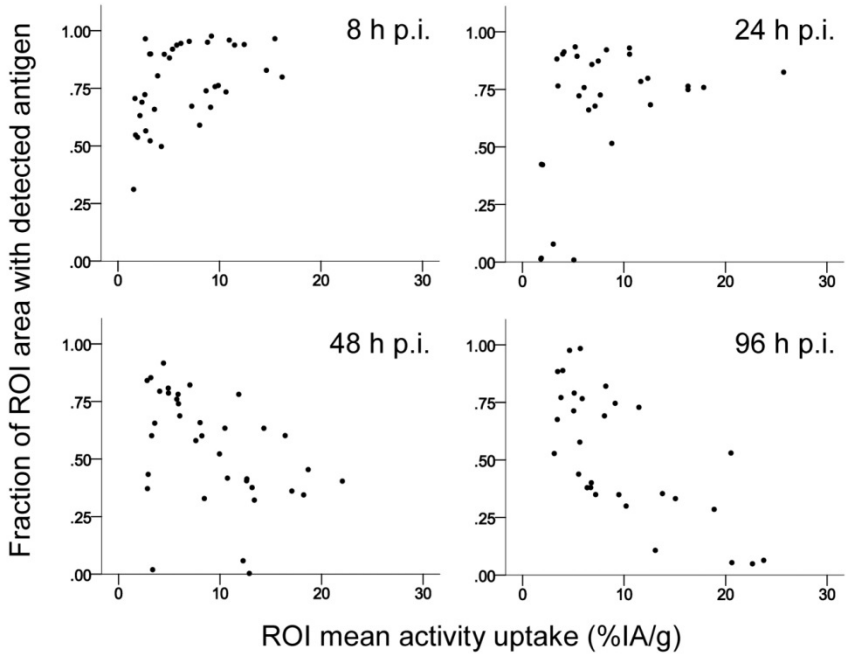

FIGURE 3. Scatter plots demonstrating the changing correlation between antigen expression and activity over time.

Tables

TABLE 1. Experimental details for the two animal groups.

		Number of animals sacrificed at each time point p.i.							
Group	Injected activity (MBq/kg)	2 h	8 h	24 h	48 h	72 h	96 h	120 h	168 h
1	50	3	3	2	3	-	3	3	-
2	25	-	3	3	3	3	3	3	3

TABLE 2. Activity of ^{177}Lu-DOTA-BR96 in tumor and blood.

	Activity of ^{177}Lu-DOTA-BR96 Median (range) (%IA/g)	
Time p.i. (h)	Tumor	Blood
0		6.72 (5.82-8.70)
2	1.97 (1.54-2.13)	
8	4.37 (3.15-6.38)	4.29 (4.13-4.62)
24	6.95 (5.09-10.2)	2.81 (2.52-2.94)
48	8.43 (6.34-9.81)	2.12 (1.95-2.43)
72	14.9 (7.48-19.0)	1.81 (1.37-1.99)
96	10.6 (4.24-20.7)	1.45 (1.29-1.89)
120	7.80 (2.65-13.0)	1.56 (1.45-1.64)
168	28.3 (11.6-52.1)	1.17 (0.98-1.69)

TABLE 3. Estimated absorbed-dose rates for whole tumor sections and high- and low-uptake regions (relative to each individual section).

	Mean absorbed-dose rate for whole tumor sections Median (range) (mGy/min)		Mean absorbed-dose rate in high-uptake ROIs Median (range) (mGy/min)		Mean absorbed-dose rate for low-uptake ROIs Median (range) (mGy/min)	
Time p.i. (h)	Group 1	Group 2	Group 1	Group 2	Group 1	Group 2
2	0.10 (0.10-0.20)		0.40 (0.30-0.50)		0.10 (0.00-0.10)	
8	0.37 (0.27-0.43)	0.49 (0.40-0.52)	0.67 (0.61-1.13)	1.01 (0.70-1.31)	0.18 (0.15-0.30)	0.27 (0.15-0.37)
24	(0.54-0.79)	0.48 (0.33-0.58)	1.12 (1.09-1.81)	0.81 (0.59-1.08)	0.47 (0.14-0.51)	0.25 (0.17-0.52)
48	0.60 (0.49-0.65)	0.53 (0.46-0.60)	1.06 (0.78-1.35)	0.90 (0.56-1.15)	0.33 (0.21-0.67)	0.28 (0.22-0.51)
72		0.71 (0.29-0.84)		1.43 (0.51-1.65)		0.27 (0.17-0.77)
96	0.43 (0.25-1.04)	0.39 (0.38-0.63)	0.78 (0.48-1.03)	0.93 (0.70-1.17)	0.23 (0.18-0.35)	0.35 (0.19-0.53)
120	0.38 (0.30-0.66)	0.37 (0.34-1.88)	0.78 (0.56-1.43)	0.79 (0.45-3.62)	0.23 (0.17-0.34)	0.29 (0.17-2.92)
168		1.10 (0.76-2.40)		1.73 (1.23-5.31)		0.52 (0.17-3.01)

TABLE 4. Pearson correlation coefficients for activity uptake and absorbed-dose rate at the time of sacrifice vs. antigen-positive area fraction in ROIs of tumor sections.

Time p.i. (h)	Pearson correlation coefficient	
	Antigen vs. activity uptake	Antigen vs. absorbed-dose rate at the time of sacrifice
8	0.450*	0.568†
24	0.384*	0.405*
48	-0.432*	-0.490*
96	-0.711†	-0.643†
120	-0.621†	-0.572†

*$p < 0.05$

†$p < 0.001$